International Journal of Robotics and Control Systems
Vol. 5, No. 2, 2025, pp. 1065-1082
ISSN 2775-2658
http://pubs2.ascee.org/index.php/ijrcs

Hierarchical Cascaded Takagi-Sugeno Model Predictive Control for Performance Enhancement of Doubly-fed Induction Generator-Based Wind Turbine Systems

Amira Aggoune [a,1,*], Farid Berrezzek [a,2], Khaled Khelil [a,3]

[a] Laboratory of Electrical Engineering and Renewable Energy, Department of Electrical Engineering, Faculty of Sciences and Technology, University of Souk Ahras, Souk Ahras, Algeria
[1] a.aggoune@univ-soukahras.dz; [2] f.berrezzek@univ-soukahras.dz; [3] khaled.khelil@univ-soukahras.dz
* Corresponding Author

ARTICLE INFO

Article history
Received February 02, 2025
Revised March 31, 2025
Accepted April 23, 2025

Keywords
Doubly-Fed Induction Generator;
Takagi-Sugeno Fuzzy Logic Controller;
Finite Control Set Model Predictive Controller;
Maximum Power Point Tracking;
Rotor Side Converter;
Output Power Quality

ABSTRACT

This paper proposes a cascaded Takagi-Sugeno Model Predictive Controller (TS-MPC) for a Doubly-fed Induction Generator (DFIG) based Wind Power Conversion System (WPCS) to maximize power extraction, maintain zero stator reactive power, and enhance power quality. For this purpose, the Takagi-Sugeno Fuzzy Logic Control (TS-FLC) is arranged in a sequential configuration with the Finite Control-Set Model Predictive Control (FCS-MPC) strategy to enhance the overall performance of the wind power system. The introduced control technique, which is applied to govern the Rotor Side Converter (RSC) of the DFIG, consists of two cascaded control loops for achieving Maximum Power Point Tracking (MPPT). The innermost control loop is implemented to regulate the d-q axis rotor currents using FCS-MPC strategy. Meanwhile the outermost control loop is employed to regulate the DFIG's rotational speed pursuant to the Tip Speed Ratio MPPT (TSR-MPPT) control framework using the TS-FLC, thus improving the predictive accuracy and control effectiveness. To validate the performance of the devised control scheme, a numerical simulation of a 1.5MW DFIG based WPCS was conducted using MATLAB/Simulink software. The simulation results demonstrate that the proposed cascaded TS-MPC not only outperforms the cascaded PI-MPC in terms of superior adaptability to nonlinearities and varying wind conditions—thanks to the inherent flexibility of TS-FLC—but also in various performance metrics, including response time, steady-state error, and total harmonic distortion (THD).Furthermore, while FCS-MPC approaches are often criticized for computational complexity, the TS-FLC structure enhances real-time feasibility by reducing computational overhead compared to conventional FLC methods. These findings reinforce the practical viability of TS-MPC for large-scale wind energy applications and indicate the effectiveness of the proposed control scheme.

This is an open-access article under the CC–BY-SA license.

1. Introduction

Nowadays, the world energy industry is witnessing a significant transition to renewable energy sources, driven by the crucial need to meet global energy demand, reduce reliance on fossil fuels, mitigate climate change and secure a sustainable energy future. Among the various renewable energy

options, wind power conversion systems (WPCS) stand out as one of the most competitive and rapidly growing alternatives [1], [2].

Wind turbines equipped with doubly-fed induction generators (DFIG) are a promising technology in modern WPCS owing to their unique features and capabilities. DFIG allows for variable-speed operation, which enables the wind turbine to operate efficiently across a wide range of wind speeds, thus maximizing energy capture. The partial-scale power converter used in DFIG is also more cost-effective compared to full-scale converters required in other turbine technologies [3]-[5]. Moreover, DFIG can deliver stable and continuous power to the grid, reducing the stress on electrical infrastructure and improving the reliability of the energy supply [6]-[10].

Since the optimal performance of a DFIG based wind turbine system relies heavily on precise and appropriate control mechanisms, numerous control strategies have been discussed in literature. One of the most popular control techniques in this context is the decoupled vector control based on PI regulators [11]. Despite its simplicity, perfect ability to decouple active and reactive powers, and straightforward design, it may struggle with dynamic changes and non-linearities inherent in DFIG system, especially under real-world conditions such as sudden wind gusts, turbulence, and grid voltage fluctuations. These challenges can result in slower response times, reduced power tracking accuracy, and potential instability, limiting the effectiveness of conventional PI controllers in practical wind energy applications [12], [13]. To overcome these drawbacks, several advanced algorithms have been discussed and developed. The sliding mode control (SMC) theory has been widely utilized in the control of wind turbine systems due to its remarkable robustness regardless the presence of system uncertainties and external disturbances [2], [14]. However, one significant drawback of SMC is the chattering phenomenon, which can damage the quality of the energy injected into the power grid [15]. In practical wind energy systems, chattering-induced high-frequency oscillations can accelerate mechanical wear, shorten the lifespan of turbine components, and reduce overall energy conversion efficiency, making SMC less suitable for long-term reliable operation [4], [16]. To address this issue, several papers have proposed enhancements to the traditional SMC strategy, including the development of second-order, third-order and integral SMC schemes [17]-[19]. Although the aforementioned strategies have improved the current waveforms delivered to the power grid, other methods, such as backstepping control, can achieve even better THD performance [20]. Backstepping control is a robust control technique recognized for managing the DFIG's issues. It also allows for precise control of both active and reactive power adjusting to changes in the turbine's maximum power output, which improves the overall power quality and efficiency of the wind turbine [21], [22]. Nevertheless, the design and implementation of backstepping controllers are complex and computationally demanding, requiring precise system modeling and extensive computational resources. In real-world wind energy applications, uncertainties in system parameters, unmodeled dynamics, and external disturbances can further complicate implementation, making backstepping control less practical for large-scale or real-time operations [23]. For that reason, fuzzy logic control (FLC) has been adopted by researchers thanks to its robustness to disturbances, adaptability to changing conditions, and ability to provide effective control without requiring an accurate mathematical model of the system [11], [24]. Generally, FLCs are primarily classified according to the structure of their rule base and the type of output they generate into two main types: Mamdani and Takagi-Sugeno (TS-FLC) [25]. In the context of the current study, TS-FLCS are often preferred over Mamdani FLCs, mainly for their high computational efficiency, which is critical for real-time control applications in wind turbine systems [26].

Recently, the Takagi-Sugeno fuzzy logic controller (TS-FLC) has gained significant research interest for improving DFIG control, enhancing the reliability and efficiency of WPCS. Studies have demonstrated its effectiveness in tracking performance, optimizing power extraction under varying conditions, and improving pitch angle control for power stability and mechanical stress reduction [26]-[29]. Additionally, adaptive neuro-fuzzy inference system-based MPPT controllers have been explored for DFIG-based wind turbines [30].

Simultaneously, Finite Control Set Model Predictive Control (FCS-MPC) has emerged as a promising approach, leveraging predictive models to optimize control actions. Research has focused on time-optimal binary linear programming for rotor-side converter (RSC) control [31], predictive rotor current and voltage control for MPPT and robustness [32]-[34], and sensorless predictive control to minimize computation time and switching losses [35]. Furthermore, integrating FCS-MPC in both RSC and grid-side converter (GSC) control loops has shown improvements in dynamic performance and power quality [36].

Previous research on TS-FLC and FCS-MPC has laid a robust foundation for their application in the control of WPCS based on DFIG, each bringing unique strengths to the table. However, there remains a gap in integrating them within a cascaded framework that leverages the strengths of both approaches while mitigating their limitations, thus enhancing overall system performance. Building on these insights, the current study explores a novel hybrid control scheme in which the TS-FLC and FCS-MPC are arranged in series configuration, thereby enhancing the efficiency and applicability in real-world scenarios. The so-called cascaded Takagi-Sugeno Model Predictive Controller (TS-MPC) is adopted to improve the overall efficiency and responsiveness by ensuring that the control decisions are processed step-by-step, with each stage refining the outcome based on the preceding stage results. Accordingly, the TS-FLC is employed to regulate the rotational speed of the DFIG in alignment with the Tip Speed Ratio Maximum Power Point Tracking (TSR-MPPT) control framework. This choice leverages the reliability and robustness of fuzzy logic to ensure precise and adaptive speed control under varying operational conditions. Simultaneously, the FCS-MPC is utilized to manage the output active and reactive powers of the DFIG. By integrating these two sophisticated control techniques, the system achieves optimal performance, maintaining stability and efficiency in power generation and distribution. The TS-FLC effectively handles the nonlinearities and uncertainties in the speed control, while the FCS-MPC provides accurate and dynamic control of power outputs, ensuring that the DFIG operates at its best performance across different operating modes. While the hybrid approach enhances robustness and predictive accuracy, concerns about computational complexity and real-time implementation remain. However, the TS-FLC's use of linear consequents reduces computational overhead, while the structured integration of FCS-MPC ensures predictive benefits without excessive demands. This balanced design makes the proposed TS-MPC both practical and effective for large-scale wind energy applications.

The remainder of this paper is organized as follows: Mathematical description of the major parts of the WPCS is presented in Section 2. Proposed cascaded TS-MPC design is the subject of Section 3. A detailed description of the FCS-MPC control technique is provided in Section 4. Section 5 provides numerical simulations to assess the effectiveness of the proposed control strategy. Finally, the conclusions of the study are drawn in Section 6.

2. DFIG-Based Wind Power Conversion System Principles

The standard structure of a WPCS consists of three-blade wind turbines that capture the kinetic energy of the wind and convert it into electrical power using DFIG. The DFIG is a three-phase induction machine adapted to operate as a generator, with both its stator and rotor electrically connected. The stator winding is directly connected to the grid, while the rotor winding is fed through bidirectional back-to-back power converters linked via a DC bus capacitor. These converters are typically designated as the grid side converter (GSC) and the rotor side converter (RSC) due to their positions relative to the grid and rotor (see Fig. 1) [3], [37].

2.1. Aerodynamic Modelling of the Wind Turbine

The aerodynamic power extracted by the wind turbine system is expressed as follows [20]:

$$P_{aero} = \frac{1}{2} C_p(\lambda, \beta) \rho \pi R^2 v^3 \quad (1)$$

Where ρ is the air density, R is the rotor turbine's radius, and v is the wind speed. C_p is the power coefficient of the wind turbine which can be expressed in terms of the blade tip ratio (TSR) λ and the pitch angle β as follows:

$$\begin{cases} C_p(\lambda,\beta) = 0.5176\left(\frac{116}{\lambda_i} - 0.4\beta - 5\right)e^{-\frac{21}{\lambda_i}} + 0.0068\lambda \\ \frac{1}{\lambda_i} = \frac{1}{\lambda + 0.008\beta} - \frac{0.035}{\beta^3 + 1} \end{cases} \quad (2)$$

The TSR is the ratio between the linear tip speed of the blades and the real wind velocity:

$$\lambda = \frac{\omega_{tur} R}{v} \quad (3)$$

Where ω_{tur} represents the turbine rotational speed. The relationship between ω_{tur} and the DFIG rotational speed ω_m in a wind turbine system is defined by the gearbox ratio G and is expressed as follows [11]:

$$\omega_{tur} = \frac{\omega_m}{G} \quad (4)$$

Accordingly, the TSR can be derived from (3) and (4):

$$\lambda = \frac{\omega_m R}{Gv} \quad (5)$$

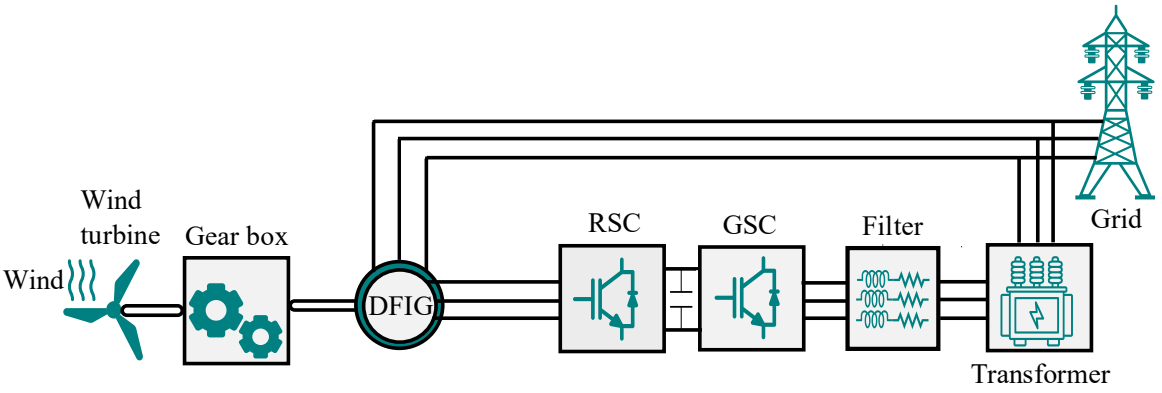

Fig. 1. The standard configuration of a WPCS fitted with DFIG

2.2. TSR-MPPT Control Algorithm

It is well known that the wind power has an intrinsic fluctuating and unexpected nature [3]. Thus, implementing the MPPT control algorithm is essential for more efficient and reliable wind power conversion. The TSR-MPPT algorithm is one of several MPPT control methods used in WPCS to optimize power output. It is an intuitive technique derived from the fundamental characteristics of the wind system [38]. From the power coefficient curve as a function of TSR for various pitch angles (Fig. 2), the maximum value is $C_{p\max} = 0$. This indicates that optimal operating conditions for peak WECS efficiency occur at $\beta = 0°$ and $\lambda_{opt} = 8.1$. Consequently, according to (3), maintaining the optimal TSR for maximum power extraction is achieved by regulating the rotational speed of the DFIG to track its reference trajectory given by:

$$\omega_m^{opt} = \frac{Gv}{R}\lambda_{opt} \quad (6)$$

Fig. 3 depicts the schematic representation of the turbine with the TSR-MPPT technique based on PI controllers, that is implemented to regulate the DFIG's rotational speed. Generally, PI controller gains are tuned by linearizing the system model around a single operating point. While this technique simplifies the tuning process, it fails to account for the various operating conditions under which WPCS may operate, causing significant fluctuations in the power coefficient C_p. This can result in suboptimal performance, highlighting the need for more advanced control strategy that can adapt to varying operating conditions. Thus, this work focuses on developing a Takagi-Sugeno fuzzy logic controller (TS-FLC) based TSR-MPPT algorithm for a DFIG-equipped wind turbine system. The proposed approach aims to enhance MPPT performance while improving output power quality, providing a cleaner reference signal for the electrical regulation loop and ensuring a more stable power supply.

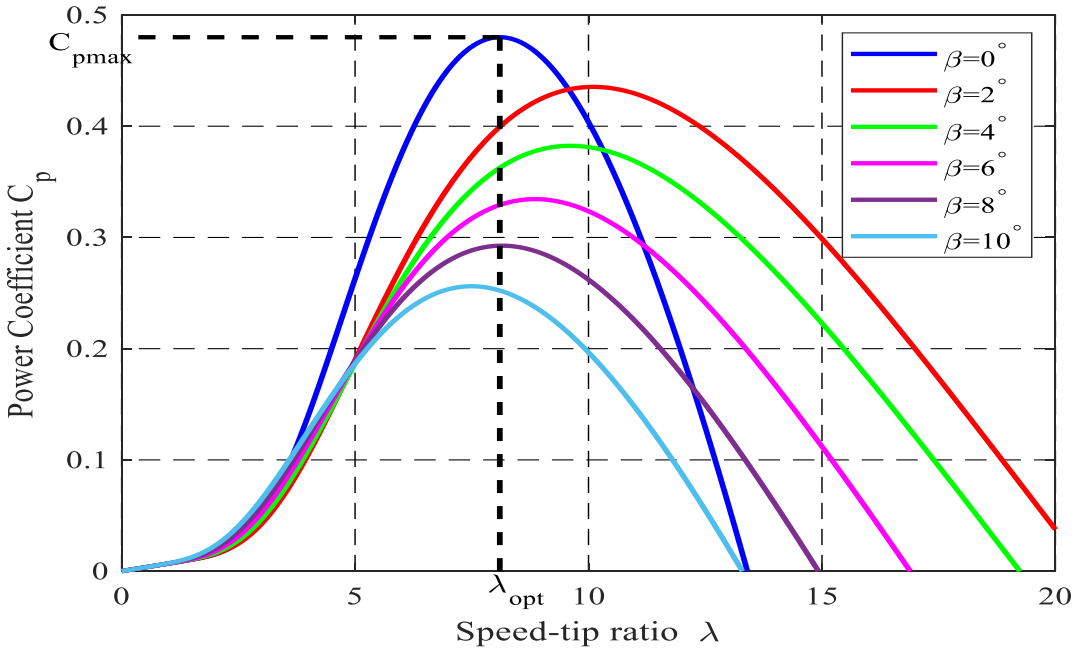

Fig. 2. Curve plot of the turbine's power coefficient as a function of the TSR and β

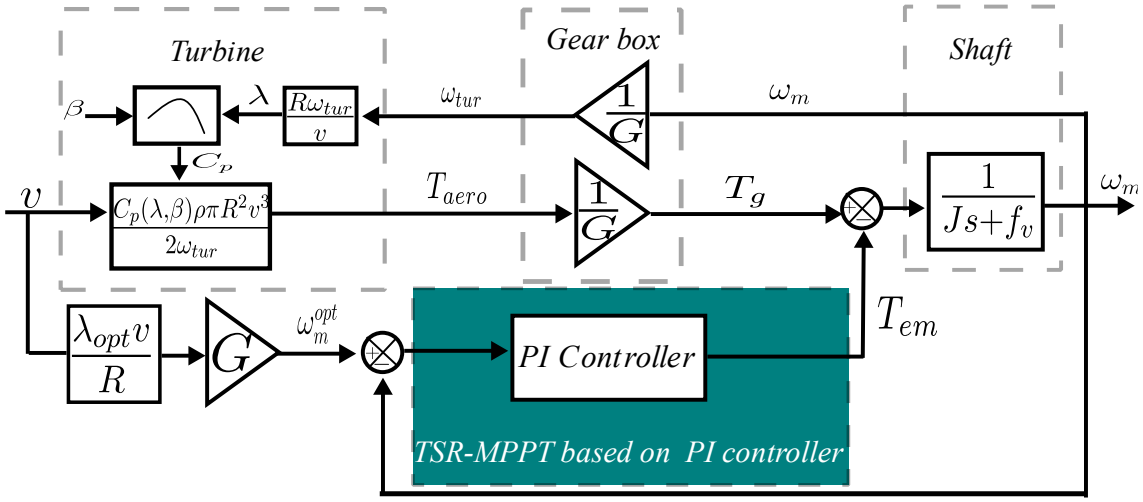

Fig. 3. The turbine schematic representation with the PI-based TSR-MPPT technique

2.3. DFIG Modelling

In the synchronous (d-q) reference frame, the dynamic model of the DFIG can be derived from its voltage and flux linkage equations as follows [30]:

$$\begin{cases} V_{sd} = R_s i_{sd} + \dfrac{d\varphi_{sd}}{dt} - \omega_s \varphi_{sq} \\ V_{sq} = R_s i_{sq} + \dfrac{d\varphi_{sq}}{dt} + \omega_s \varphi_{sd} \\ V_{rd} = R_r i_{rd} + \dfrac{d\varphi_{rd}}{dt} - g\omega_s \varphi_{rq} \\ V_{rq} = R_r i_{rq} + \dfrac{d\varphi_{rq}}{dt} + g\omega_s \varphi_{rd} \end{cases} \tag{7}$$

$$\begin{cases} \varphi_{sd} = L_s i_{sd} + L_m i_{rd} \\ \varphi_{sq} = L_s i_{sq} + L_m i_{rq} \\ \varphi_{rd} = L_r i_{rd} + L_m i_{sd} \\ \varphi_{rq} = L_r i_{rq} + L_m i_{sq} \end{cases} \tag{8}$$

Where the subscripts sd/rd and sq/rq indicate the d-axis and q-axis components of the stator/ rotor voltage V, current i, and flux linkage φ, respectively. R_s, R_r are the stator and rotor resistances, while L_s, L_r, L_m refer to stator, rotor and mutual inductances respectively. Additionally, ω_s, g are the stator angular speed and generator slip respectively.

The mechanical dynamic of the DFIG is described by the equation of motion which relates the electromagnetic torque T_{em} and the mechanical torque T_g to the DFIG rotational speed, the WPCS total inertia J, and the viscous friction f_v, in accordance with Newton's second law, as expressed below [3]:

$$J\frac{d\omega_m}{dt} + f_v\omega_m = T_g - T_{em} \tag{9}$$

The expression of the electromagnetic torque can be provided by the following formula [36]:

$$T_{em} = \frac{3}{2}\frac{pL_m}{L_s}\left(i_{sq}\varphi_{sd} - i_{sd}\varphi_{sq}\right) \tag{10}$$

The stator active and reactive powers of the DFIG are defined as [11]:

$$\begin{cases} P_s = \dfrac{3}{2}(V_{sd}i_{sd} + V_{sq}i_{sq}) \\ Q_s = \dfrac{3}{2}(V_{sq}i_{sd} - V_{sd}i_{sq}) \end{cases} \tag{11}$$

Under ideal grid voltage conditions, the amplitude and velocity of the stator flux can be considered constant. Moreover, for medium and large wind power generators, the stator resistance can be neglected. by aligning the d-axis of the reference frame to the stator flux, the stator voltage expressions can be derived from (5) as follows:

$$V_{sd} = \varphi_{sq} = 0, \qquad V_{sq} = V_s = \omega_s\varphi_s \tag{12}$$

Consequently, the stator currents could be obtained from (2) as follows:

$$\begin{cases} i_{sd} = \dfrac{\varphi_s}{L_s} - \dfrac{L_m}{L_s}i_{rd} \\ i_{sq} = -\dfrac{L_m}{L_s}i_{rq} \end{cases} \tag{13}$$

Finally, substituting equations (7) and (6) into (5), the stator active and reactive power are expressed by:

$$\begin{cases} P_s = -\frac{3}{2}\frac{V_s L_m}{L_s} i_{rq} \\ Q_s = -\frac{3}{2}\left(\frac{V_s L_m}{L_s} i_{rd} - \frac{V_s^2}{\omega_s L_s}\right) \end{cases} \quad (14)$$

From (14), it is evident that the active power is regulated through the q-axis rotor current, whereas the reactive power is controlled via the d-axis rotor current.

2.4. Rotor Side Converter (RSC) Modeling

The rotor side converter (RSC), typically implemented as a 2-level power converter in a DFIG based wind turbine system, is responsible for controlling the rotor currents to regulate both active and reactive power. The output voltage generated by a 2-level RSC is expressed as:

$$\begin{bmatrix} V_{An} \\ V_{Bn} \\ V_{Cn} \end{bmatrix} = \frac{V_{dc}}{3} \begin{bmatrix} 2 & -1 & -1 \\ -1 & 2 & -1 \\ -1 & -1 & 2 \end{bmatrix} \begin{bmatrix} S_a \\ S_b \\ S_c \end{bmatrix} \quad (15)$$

Here, V_{An}, V_{Bn}, V_{Cn} represent the phase voltages, V_{dc} denotes the DC-link voltage, and S_a, S_b, S_c are the switching states of the RSC. Note that for a two-level RSC, there are a total of eight possible switching states, resulting in eight distinct voltage vectors as shown in Fig. 4.

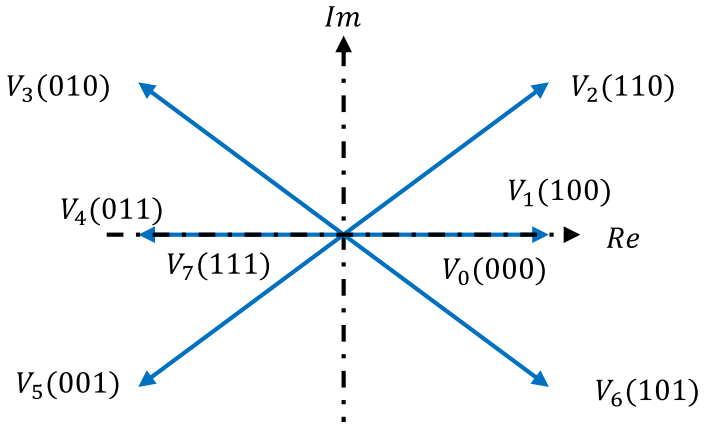

Fig. 4. Possible voltage vectors for the RSC

3. Formulation of the Control Problem for DFIG-Based WPCS

An effective control strategy for a DFIG-based wind turbine system must account for several critical challenges, including the inherent nonlinearity of the DFIG, the intermittent and unpredictable nature of wind power, system uncertainties, and the quality of the generated electrical power. The nonlinear characteristics of the DFIG arise from its complex dynamic interactions, making conventional control techniques less effective under varying operating conditions. Additionally, wind speed fluctuations introduce continuous variations in power generation, requiring a robust control approach to ensure stability and optimal energy extraction. System uncertainties, such as parameter variations and external disturbances, further complicate control design and can impact performance if not properly addressed. Moreover, maintaining high power quality by minimizing total harmonic distortion (THD) and reactive power fluctuations is essential for seamless grid integration. To tackle these challenges, the proposed cascaded TS-MPC leverages the adaptability of Takagi-Sugeno fuzzy logic combined with predictive control, ensuring improved dynamic response, enhanced robustness, and better power quality under real-world operating conditions. While the hybrid approach improves robustness and predictive accuracy, challenges related to computational complexity and real-time implementation persist. However, the TS-FLC's linear consequents help minimize computational overhead, while the structured integration of FCS-MPC retains predictive advantages without

imposing excessive computational demands. This well-balanced design ensures that the proposed TS-MPC remains both practical and efficient for large-scale wind energy applications.

4. Proposed TSR-MPPT Based TS-FLC Technique

4.1. TS-FLC Theory Basics

The Takagi-Sugeno fuzzy logic controller (TS-FLC) theory was initially introduced by Takagi and Sugeno in 1985. It is a type of fuzzy inference system that uses a combination of fuzzy rules and polynomial equations, in the antecedent and consequent part respectively, to map inputs to outputs [39]. Compared with the Mamdani FLC, the TS-FLC offers a variety of features including suitability for applications requiring high precision, computational efficiency, and ease of integration with adaptive and learning algorithms [40]. The rule formula for a of a TS-FLC model rule is typically given as follows [25], [26]:

$$R^i: \begin{matrix} If\ x_1\ is\ A_1^i\ and\ x_2\ is\ A_2^i\ and\ \dots\ and\ x_j\ is\ A_j^i \\ Then\ y^i = c_1^i x_1 + c_2^i x_2 + \cdots + c_j^i x_j \end{matrix} \tag{16}$$

With R^i denotes the i^{th} fuzzy rule, A_j^i are the fuzzy sets, $i \in \{0,1,2,\dots,N\}$, and $j \in \{0,1,2,\dots,M\}$ where N and M denote the number of fuzzy rules and antecedents, respectively. c_j^i are constants parameters for inputs variables x_j and y^i is the i^{th} output rule.

In the TS-FLC, the defuzzification step is inherently achieved by the parametric nature of the output polynomial functions. Thus, the outputs of the N fuzzy rules are aggregated based on their firing fitness using the weighted average technique to derive the overall output y:

$$y = \frac{\sum_{i=1}^{N} w^i y^i}{\sum_{i=1}^{N} w^i} \tag{17}$$

Where w^i is the firing fitness of the i^{th} rule given in function of the membership degree of x_i as follows:

$$w^i(x) = \prod_{i=1}^{N} \mu_{A_j^i}(x_i) \tag{18}$$

4.2. TS-FLC Design for the DFIG's Speed Control

This part is dedicated to designing a mechanical regulation loop based on a TS-FLC strategy. The TS-FLC adapts to varying wind conditions through its rule-based structure, allowing real-time adjustments to the control strategy without requiring an explicit mathematical model of the system's nonlinearities. Unlike PI controllers, which often require gain scheduling to adapt to changing wind speeds, the TS-FLC inherently accommodates system variations without complex tuning, thereby enhancing both efficiency and reliability in wind power applications. The proposed regulator aims to control the DFIG's rotational speed to track its optimal reference trajectory, as defined by (6), in order to ensure maximum power extraction for the WPCS. The proposed TS-FLC regulates the DFIG speed through the control of the electromagnetic torque. Therefore, the DFIG's rotational speed tracking error $e_{\omega_m}(t)$ as well as its error change $\Delta e_{\omega_m}(t)$ are selected as fuzzy input variables, with the output being the DFIG's electromagnetic torque (see Fig. 5). Consequently, the input control variables could be defined by:

$$\begin{cases} e_{\omega_m}(t) = \omega_m^{opt}(t) - \omega_m(t) \\ \Delta e_{\omega_m}(t) = e_{\omega_m}(t) - e_{\omega_m}(t-1) \end{cases} \tag{19}$$

The fuzzy inference system has been developed to effectively manage the DFIG's high nonlinearity and wind power intermittent nature, ensuring optimal performance and stability for the WPCS. The fuzzy parameters selection phase and the tuning process have been carried out manually based on empirical observations and expert knowledge, prioritizing simplicity and high precision. Thus, the universe of discourse for each control variable is split into three fuzzy subsets using three Gaussian membership functions (MFs), as depicted in Fig. 6. Each fuzzy input variable is associated with three MFs, labelled as Negative "NE", Zero "ZE" and Positive "PO", reflecting the controller's flexibility and adaptability to different operation ranges. Moreover, the rule base is composed of 3 × 3 rules. These rules govern the decision-making mechanism, providing a systematic framework for interpreting the DFIG's speed tracking error dynamics and producing corresponding electromagnetic torque output actions. Each rule represents a distinct condition or scenario based on the wind turbine system's behavior and operational requirements (see Table 1). For instance:

- If both e_{ω_m} and Δe_{ω_m} are NE, the rule defines T_{em} adjustment that acts to counteract the negative error, driving the speed closer to the reference value.
- If e_{ω_m} is NE and Δe_{ω_m} is ZE, T_{em} should be increased proportionally to e_{ω_m} to correct the error while maintaining a steady response.
- If e_{ω_m} is ZE and Δe_{ω_m} is PO, the cell defines T_{em} adjustment that smooths the system response, preventing overshooting.

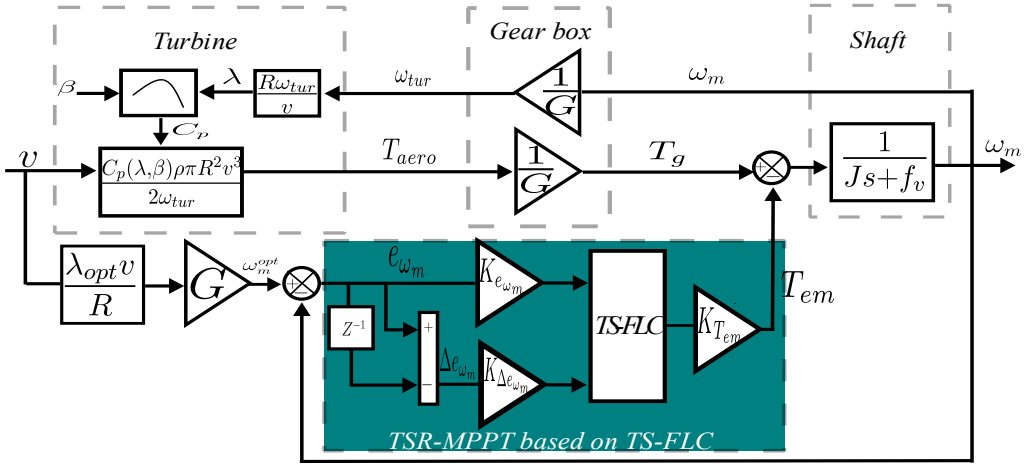

Fig. 5. The turbine schematic representation with the TS-FLC based TSR-MPPT technique

As a result, the total output value is given by the following:

$$T_{em} = \frac{\sum_{i=1}^{9} w^i T_{em}^i}{\sum_{i=1}^{9} w^i} \tag{20}$$

Table 1. Fuzzy Rules

T_{em}		e_{ω_m}		
		NE	**ZE**	**PO**
Δe_{ω_m}	**NE**	$T_{em}^1 = \alpha_1 e_{\omega_m} + \beta_1 \Delta e_{\omega_m} + \gamma_1$	$T_{em}^2 = \alpha_1 e_{\omega_m} + \beta_1 \Delta e_{\omega_m} + \gamma_1$	$T_{em}^3 = \alpha_2 e_{\omega_m} + \beta_2 \Delta e_{\omega_m} + \gamma_2$
	ZE	$T_{em}^4 = \alpha_1 e_{\omega_m} + \beta_1 \Delta e_{\omega_m} + \gamma_1$	$T_{em}^5 = \alpha_2 e_{\omega_m} + \beta_2 \Delta e_{\omega_m} + \gamma_2$	$T_{em}^6 = \alpha_2 e_{\omega_m} + \beta_2 \Delta e_{\omega_m} + \gamma_2$
	PO	$T_{em}^7 = \alpha_2 e_{\omega_m} + \beta_2 \Delta e_{\omega_m} + \gamma_2$	$T_{em}^8 = \alpha_3 e_{\omega_m} + \beta_3 \Delta e_{\omega_m} + \gamma_3$	$T_{em}^9 = \alpha_4 e_{\omega_m} + \beta_4 \Delta e_{\omega_m} + \gamma_4$

Note that $\alpha_1, \alpha_2, \alpha_3, \alpha_4$ represent the scaling factors of e_{ω_m}, while $\beta_1, \beta_2, \beta_3, \beta_4$ correspond to the scaling factors of Δe_{ω_m}. $\gamma_1, \gamma_2, \gamma_3, \gamma_4$ represent bias terms added to the outputs of the respective rules.

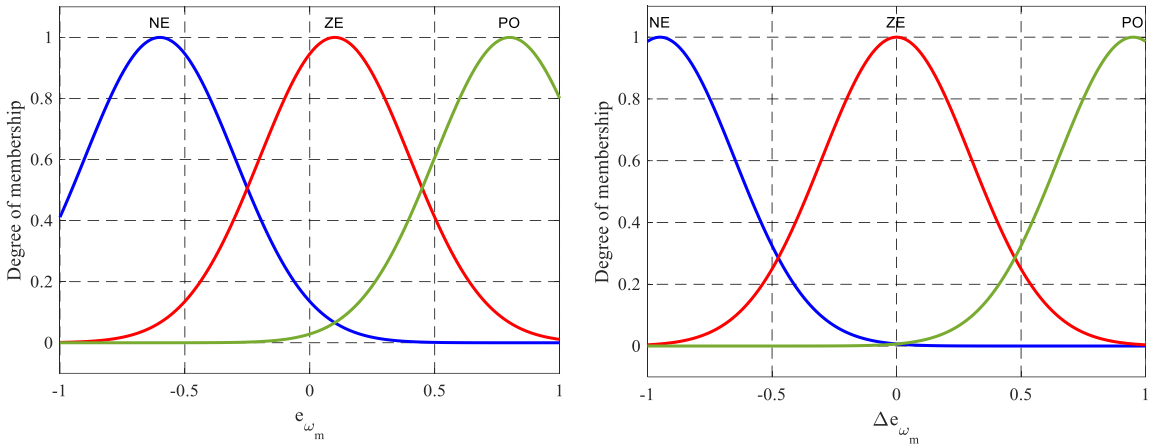

Fig. 6. MFs distribution for the TS-FLC inputs

5. Finite Control Set Model Predictive Control Approach Applied to DFIG-Based WPCS

Finite control-set model predictive control (FCS-MPC) has become an efficient and reliable approach, gaining recognition as a promising alternative for managing nonlinear systems in recent years. By leveraging the dynamic model of the process, FCS-MPC predicts future behavior and optimizes control inputs over a short time horizon, aiming to minimize an objective function that determines the suitable voltage vector to apply during each switching period [32], [36]. Fig. 7 illustrates the typical scheme of FCS-MPC, which consists of four main blocks [41]:

- **References estimation:** This step consists in defining the reference control values $x^{ref}(k)$ to be imposed to the system. In this study the reference control variables are the rotor currents that can be derived from (14) as follows:

$$\begin{cases} i_{rq}^{ref} = -\dfrac{2}{3}\dfrac{L_s}{V_s L_m} P_s^{ref} \\ i_{rd}^{ref} = -\dfrac{2}{3}\dfrac{L_s}{V_s L_m} Q_s^{ref} + \dfrac{V_s}{\omega_s L_m} \end{cases} \tag{21}$$

- **Extrapolation:** The future values of the reference-controlled variables $x^{ref}(k+1)$ are calculated using the current and previous sample values $x^{ref}(k)$, $x^{ref}(k-1)$, $x^{ref}(k-2)$…, through the application of second-order Lagrange extrapolation:

$$x^{ref}(k+1) = 3x^{ref}(k) - 3x^{ref}(k-1) + x^{ref}(k-2) \tag{22}$$

- **Predictive model:** This technique leverages the dynamic model of the system to explicitly forecast the future states, denoted as $x(k+1)$. The predictive model is discretized employing the forward difference Euler method, transforming the continuous-time model into a discrete-time approximation, as detailed in (23):

$$\frac{dx}{dt} = \frac{x(k+1) - x(k)}{T_s} \tag{23}$$

- **Objective function minimization:** In this step of the FCS-MPC process, the error between the predicted control variables and the extrapolated reference values is evaluated using the error function, as shown in (24):

$$g(k) = \left(x^{ref}(k+1) - x(k+1)\right)^2 \tag{24}$$

This function quantifies the discrepancy between the desired reference state $x^{ref}(k+1)$ and the predicted state $x(k+1)$. The control algorithm then assesses all possible switching states of the static converter, identifying the state that minimizes this error. The switching state that produces the least error is selected and applied to the static converter during the next sampling period, ensuring that the system operates as closely as possible to the desired reference trajectory.

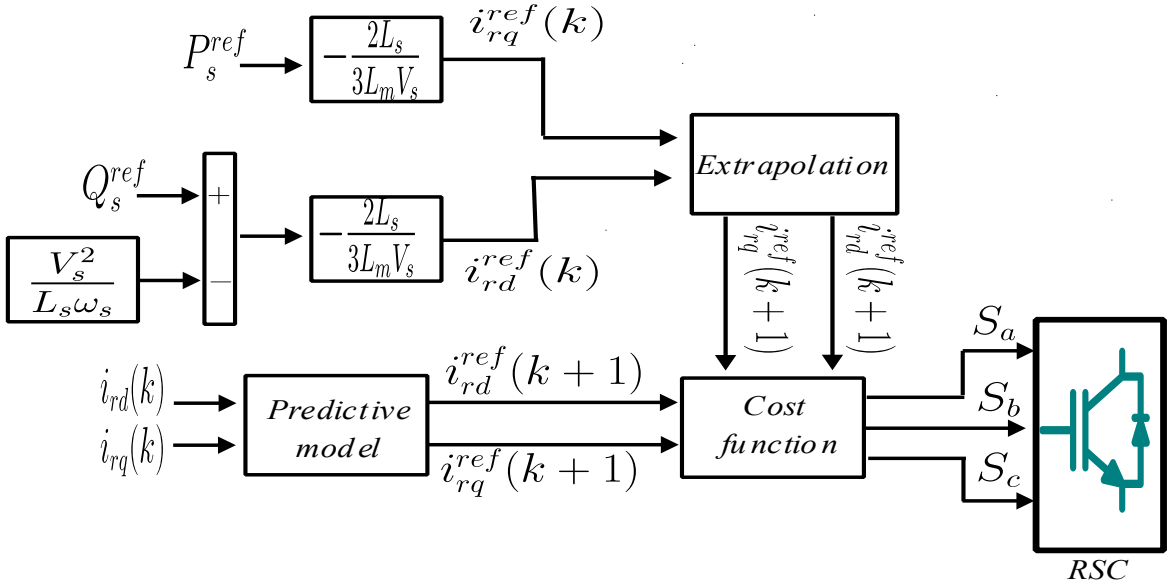

Fig. 7. Typical structure of the FCS-MPC

5.1. Current Predictive Control for the RSC

In the synchronous (d-q) reference frame, the continuous-time state-space representation of DFIG's rotor currents is given by [42]:

$$\begin{cases} \frac{di_{rd}}{dt} = \frac{L_m}{\sigma}\left(\frac{1}{\tau_s L_r} i_{sd} - \frac{\omega_s \kappa_s}{L_r} i_{sq} - \frac{1}{\tau_r L_m} i_{rd} + \omega_s \kappa_g i_{rq} - \frac{1}{L_s L_r} V_{sd} + \frac{1}{L_r L_m} V_{rd}\right) \\ \frac{di_{rq}}{dt} = \frac{L_m}{\sigma}\left(\frac{\omega_s \kappa_s}{L_r} i_{sd} + \frac{1}{\tau_s L_r} i_{sq} - \omega_s \kappa_g i_{rd} - \frac{1}{\tau_r L_m} i_{rq} - \frac{1}{L_s L_r} V_{sq} + \frac{1}{L_r L_m} V_{rq}\right) \end{cases} \quad (25)$$

With: $\begin{cases} \kappa_g = \left(\frac{g}{L_m} - \frac{L_m}{L_s L_r}\right) \\ \kappa_s = (1-g) \\ \tau_s = \frac{L_s}{R_s}, \tau_r = \frac{L_r}{R_r} \end{cases}$

By discretizing the d-q axis rotor current expressions using (23), the predictive model is then described as follows:

$$\begin{cases} i_{rd}(k+1) = \frac{L_m T_s}{\sigma}\left(\left(1 - \frac{1}{\tau_r L_m}\right) i_{rd}(k) + \omega_s \kappa_g i_{rq}(k) + \frac{1}{\tau_s L_r} i_{sd}(k) - \frac{\omega_s \kappa_s}{L_r} i_{sq}(k) - \frac{1}{L_s L_r} V_{sd}(k) + \frac{1}{L_m L_r} V_{rd}(k)\right) \\ i_{rq}(k+1) = \frac{L_m T_s}{\sigma}\left(\left(1 - \frac{1}{\tau_r L_m}\right) i_{rq}(k) - \omega_s \kappa_g i_{rd}(k) + \frac{\omega_s \kappa_s}{L_r} i_{sd}(k) + \frac{1}{\tau_s L_r} i_{sq}(k) - \frac{1}{L_s L_r} V_{sq}(k) + \frac{1}{L_m L_r} V_{rq}(k)\right) \end{cases} \quad (26)$$

5.1. Objective Function Definition

In an optimization problem, the performance quality of the controlled system is evaluated by minimizing an objective function. In this case, the objective function is used to determine the optimal switching state for the next sampling period and select the voltage vector that minimizes the error. Typically, the objective function is formulated based on the system's requirements and decision variables. The rotor currents in the d-q axis are responsible for controlling the stator's reactive and active powers, respectively. Therefore, the objective function for the RSC is given by:

$$g(k) = \left(i_{rd}^{ref}(k+1) - i_{rd}(k+1)\right)^2 + \left(i_{rq}^{ref}(k+1) - i_{rq}(k+1)\right)^2 \quad (27)$$

6. Results and Discussion

This section validates the performance of the proposed cascaded TS-MPC controller for speed and power control of grid-connected variable-speed wind turbines equipped with DFIG through numerical simulations conducted in the MATLAB/Simulink environment. The parameters defining the simulated 1.5 MW wind system and the introduced controllers' parameters are indexed in Table 2 and Table 3 respectively. The performance of the proposed cascaded TS-MPC, illustrated in Fig. 8, is evaluated by comparing it to the standard cascaded PI-MPC controller. Since the primary goal of this paper is to design a controller that can handle sudden unexpected fluctuations in wind velocity, an intermittent wind speed profile is applied to the WPCS during this test, as depicted in Fig. 9. To assess the robustness of the designed TS-FLC, the controller was tested under parameter variations, specifically by altering the system's inertia and viscous friction by 150% between 0s and 2s. This evaluation aimed to examine the controller's ability to maintain stability and performance under dynamic system changes. Furthermore, the following running scenario is applied to the DFIG wind turbine system: The stator active power is set to match the maximum power produced by the wind turbine, while the stator reactive power reference is adjusted to zero to ensure the power factor remains at unity.

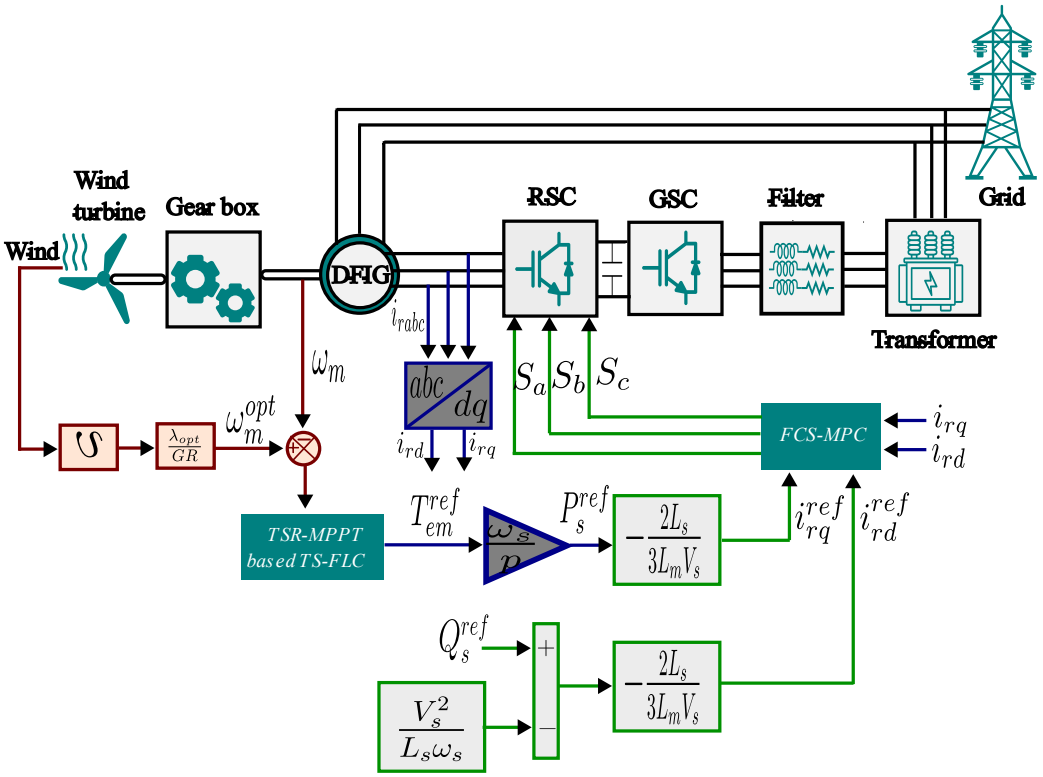

Fig. 8. Cascaded TS-MPC overall structure

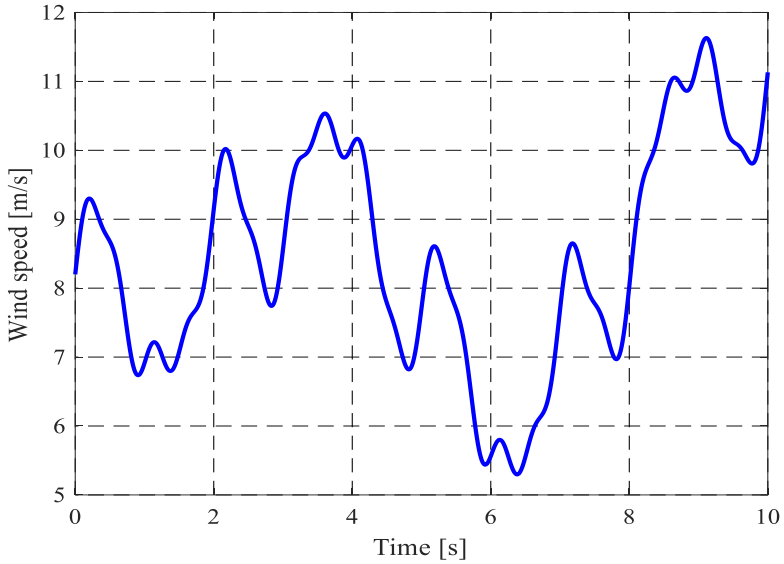

Fig. 9. The applied wind speed profile

Fig. 10 illustrates the obtained simulation results of the DFIG based WPCS for both presented strategies. Both control strategies clearly ensure the reference tracking of the DFIG rotational speed to its optimal trajectory. However, the cascaded TS-MPC still provides superior level of performance in comparison to the cascaded PI-MPC. In terms of rapidity, the cascaded TS-MPC outperforms the cascaded PI-MPC significantly. Moreover, the cascaded TS-MPC outperforms the cascaded PI-MPC in terms of accuracy and maximum power extraction as proven by keeping the power coefficient stabilized to its optimal value without fluctuations. Concerning the DFIG controlled variables, it can be clearly seen that they are quicky stabilized using the cascaded TS-MPC. The stator active power accurately tracks its reference value, corresponding to the maximum power generated by the wind turbine system. At the same time, the stator reactive power is maintained at zero throughout the simulation. From the rotor current evolution, it is evident that the d-q axis rotor currents correspond directly to the stator reactive and active powers, respectively, and effectively track their specified reference values. Table 4 presents a comparative analysis of the Cascaded TS-MPC and Cascaded PI-MPC control strategies across various key performance metrics. The results highlight the superior performance of the Cascaded TS-MPC, which exhibits noticeably faster response and settling times, achieving improvements of 62.4% and 95.5%, respectively, over the PI-MPC approach. Additionally, the steady-state error and mean squared error (MSE) are notably lower for TS-MPC, showcasing improvements of 67.3% and 64.2%, respectively, indicating higher accuracy and precision. Furthermore, the total harmonic distortion (THD) is slightly reduced for TS-MPC compared to PI-MPC, highlighting its better ability to minimize distortions. Overall, the simulation outcomes clearly demonstrate that cascaded TS-MPC consistently outperforms the cascaded PI-MPC across all performance metrics and ensure a more effective and robust control to the WPCS based on DFIG.

Table 2. System parameters

Parameter	Value/Unit	Parameter	Value/Unit
Nominal Power	1.5 MW	Rotor resistance	0.021 Ω
Stator inductance	0.0137 H	System inertia	1000 kg.m^3
Rotor inductance	0.0135 H	Viscous friction	0.024 N.m.s/rad
Mutual inductance	0.0135 H	Blade radius	35.25 m
Stator resistance	0.012 Ω	Gear box gain	70

Table 3. Cascaded TS-MPC parameters

Scaling factors of e_{ω_m}	$\alpha_1 = 1.85$	$\alpha_2 = 1.30$	$\alpha_3 = 3.70$	$\alpha_4 = 7$
Scaling factors of Δe_{ω_m}	$\beta_1 = 1.10$	$\beta_2 = 1.25$	$\beta_3 = 2.50$	$\beta_4 = 0$
Bias terms	$\gamma_1 = 4.50$	$\gamma_2 = 2.90$	$\gamma_3 = 3$	$\gamma_4 = 5$

Table 4. Comparative analysis between the proposed cascaded TS-MPC and the cascaded PI-MPC

	Cascaded TS-MPC	Cascaded PI-MPC	Improvement (%)
Response time (ms)	0.08	5.2	62.4
Settling time (ms)	1.5	34	95.5
Steady state error (%)	1.0062	3.082	67.3
MSE	1.2835	3.5898	64.2
THD (%)	0.61	0.71	14.7

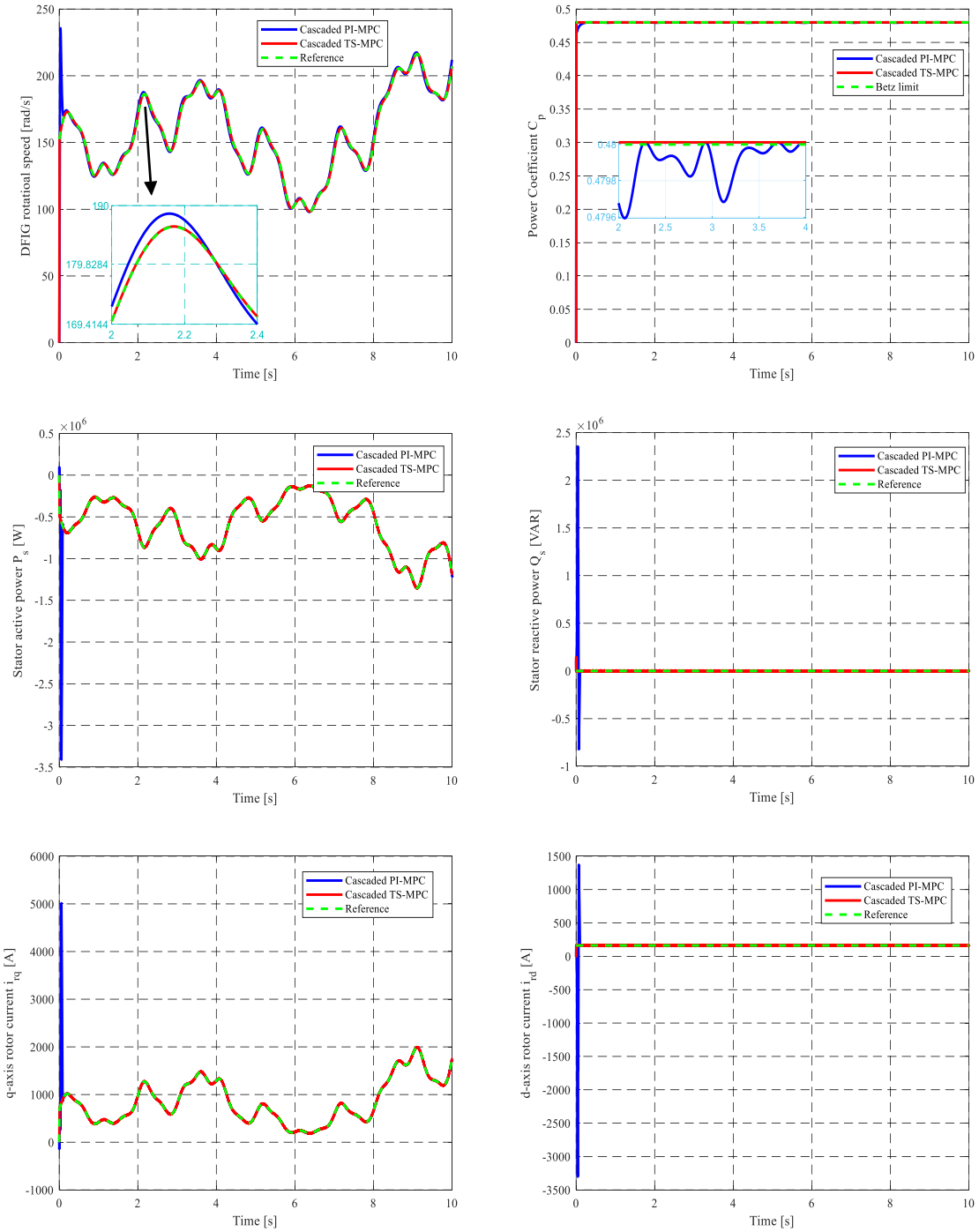

Fig. 10. The obtained results of the DFIG based WPCS

7. Conclusion

The present paper examines the control of a WPCS fitted with a DFIG utilizing a cascaded TS-MPC. The proposed control scheme integrates the TS-FLC and the FCS-MPC to enhance the performance of DFIG-based wind turbine systems. This combination results in a highly responsive and adaptive control strategy that improves the efficiency and reliability of the wind turbine system. The synergy between the fuzzy logic controller's adaptability and the predictive, optimal control of FCS-MPC ensures superior performance, especially under fluctuating wind conditions, ultimately leading to increased energy capture and reduced mechanical stress on the turbine components. The performance evaluation demonstrates the superiority of the cascaded TS-MPC over the cascaded PI-MPC, as evidenced by significant improvements in key performance metrics. The TS-MPC achieves a 62.4% improvement in response time, a 95.5% improvement in settling time, a 67.3% reduction in steady-state error, a 64.2% reduction in MSE, and a 14.7% reduction in THD. These results clearly underscore the effectiveness of the proposed control strategy in achieving superior dynamic response, increased energy capture, and enhanced overall reliability of the wind power conversion system. Although the proposed hybrid approach improves robustness and predictive accuracy, challenges related to computational complexity and real-time implementation remain. However, the use of linear consequents in TS-FLC reduces computational overhead, while the structured integration of FCS-MPC maintains predictive advantages without excessive processing demands. This balanced framework enhances the feasibility and effectiveness of the proposed TS-MPC for large-scale wind energy applications. As a future direction, integrating optimization techniques into the TS-FLC design could further enhance parameter tuning, adaptability, and overall system performance.

Author Contribution: All authors contributed equally to the main contributor to this paper. All authors read and approved the final paper.

Funding: This research received no external funding.

Conflicts of Interest: The authors declare no conflict of interest.

References

[1] I. Yaichi, A. Semmah, and P. Wira, "Control of doubly fed induction generator with maximum power point tracking for variable speed wind energy conversion systems," *Periodica Polytechnica Electrical Engineering and Computer Science*, vol. 64, no. 1, pp. 87–96, 2020, https://doi.org/10.3311/PPee.14166.

[2] J. Wang, D. Bo, Q. Miao, Z. Li, X. Wu, and D. Lv, "Maximum power point tracking control for a doubly fed induction generator wind energy conversion system based on multivariable adaptive super-twisting approach," *International Journal of Electrical Power & Energy Systems*, vol. 124, p. 106347, 2021, https://doi.org/10.1016/j.ijepes.2020.106347.

[3] A. Kasbi and A. Rahali, "Performance optimization of doubly-fed induction generator (DFIG) equipped variable-speed wind energy turbines by using three-level converter with adaptive fuzzy PI control system," *Materialstoday Proceedings*, vol. 47, pp. 2648-2656, 2021, https://doi.org/10.1016/j.matpr.2021.05.406.

[4] N. Bounar, S. Labdai, and A. Boulkroune, "PSO–GSA based fuzzy sliding mode controller for DFIG-based wind turbine," *ISA Transactions*, vol. 85, pp. 177-188, 2019, https://doi.org/10.1016/j.isatra.2018.10.020.

[5] B. Desalegn, D. Gebeyehu, and B. Tamrat, "Smoothing electric power production with DFIG-based wind energy conversion technology by employing hybrid controller model," *Energy Reports*, vol. 10, pp. 38–60, 2023, https://doi.org/10.1016/j.egyr.2023.06.004.

[6] R. Mittal, K. S. Sandhu, and D. K. Jain, "An Overview of Some Important Issues Related to Wind Energy Conversion System (WECS)," *International Journal of Environmental Science and Development*, vol. 1, no. 4, pp. 351–363, 2010, https://doi.org/10.7763/IJESD.2010.V1.69.

[7] S. Karad and R. Thakur, "Recent Trends of Control Strategies for Doubly Fed Induction Generator Based Wind Turbine Systems: A Comparative Review," *Archives of Computational Methods in Engineering*, vol. 28, no. 1, pp. 15–29, 2021, https://doi.org/10.1007/s11831-019-09367-3.

[8] S. A. Nasef, A. A. Hassan, H. T. Elsayed, M. B. Zahran, M. K. El-Shaer, and A. Y. Abdelaziz, "Optimal Tuning of a New Multi-input Multi-output Fuzzy Controller for Doubly Fed Induction Generator-Based Wind Energy Conversion System," *Arabian Journal for Science and Engineering*, vol. 47, no. 3, pp. 3001–3021, 2022, https://doi.org/10.1007/s13369-021-05946-4.

[9] A. G. Abo-Khalil, "Synchronization of DFIG output voltage to utility grid in wind power system," *Renewable Energy*, vol. 44, pp. 193–198, 2012, https://doi.org/10.1016/j.renene.2012.01.009.

[10] G. S. Kaloi, J. Wang, and M. H. Baloch, "Active and reactive power control of the doubly fed induction generator based on wind energy conversion system," *Energy Reports*, vol. 2, pp. 194-200, 2016, https://doi.org/10.1016/j.egyr.2016.08.001.

[11] O. Zamzoum, Y. El Mourabit, M. Errouha, A. Derouich, and A. El Ghzizal, "Power control of variable speed wind turbine based on doubly fed induction generator using indirect field-oriented control with fuzzy logic controllers for performance optimization," *Energy Science & Engineering*, vol. 6, no. 5, pp. 408-423, 2018, https://doi.org/10.1002/ese3.215.

[12] A. Tamaarat and A. Benakcha, "Performance of PI controller for control of active and reactive power in DFIG operating in a grid-connected variable speed wind energy conversion system," *Frontiers in Energy*, vol. 8, no. 3, pp. 371–378, 2014, https://doi.org/10.1007/s11708-014-0318-6.

[13] B. Wadawa, Y. Errami, A. Obbadi, S. Sahnoun, E. Chetouani, and M. Aoutoul, "Comparative application of the self-adaptive fuzzy-PI controller for a wind energy conversion system connected to the power grid and based on DFIG," *International Journal of Dynamics and Control*, vol. 10, no. 6, pp. 2151–2173, 2022, https://doi.org/10.1007/s40435-022-00952-2.

[14] A. M. Kassem, K. M. Hasaneen, and A. M. Yousef, "Dynamic modeling and robust power control of DFIG driven by wind turbine at infinite grid," *International Journal of Electrical Power & Energy Systems*, vol. 44, no. 1, pp. 375–382, 2013, https://doi.org/10.1016/j.ijepes.2011.06.038.

[15] A. Kasbi and A. Rahali, "Adaptive FOPI controller based on the fuzzy supervisory for wind power conversion system equipped by a doubly fed induction generator," *International Transactions on Electrical Energy Systems*, vol. 31, no. 8, pp. 1-29, 2021, https://doi.org/10.1002/2050-7038.12923.

[16] Y. E. Fadili, Y. Berrada, and I. Boumhidi, "Novel control strategy for the global model of wind turbine," *International Journal of Electrical and Computer Engineering (IJECE)*, vol. 14, no. 1, pp. 258–267, 2024, http://doi.org/10.11591/ijece.v14i1.pp258-267.

[17] B. Kelkoul and A. Boumediene, "Stability analysis and study between classical sliding mode control (SMC) and super twisting algorithm (STA) for doubly fed induction generator (DFIG) under wind turbine," *Energy*, vol. 214, p. 118871, 2021, https://doi.org/10.1016/j.energy.2020.118871.

[18] S. Kadi, H. Benbouhenni, E. Abdelkarim, K. Imarazene, and E. M. Berkouk, "Implementation of third-order sliding mode for power control and maximum power point tracking in DFIG-based wind energy systems," *Energy Reports*, vol. 10, pp. 3561-3579, 2023, https://doi.org/10.1016/j.egyr.2023.09.187.

[19] H. Chojaa, A. Derouich, S. E. Chehaidia, O. Zamzoum, M. Taoussi, and H. Elouatouat, "Integral sliding mode control for DFIG based WECS with MPPT based on artificial neural network under a real wind profile," *Energy Reports*, vol. 7, pp. 4809–4824, 2021, https://doi.org/10.1016/j.egyr.2021.07.066.

[20] C. Hamid *et al.*, "Performance improvement of the variable speed wind turbine driving a dfig using nonlinear control strategies," *International Journal of Power Electronics and Drive Systems*, vol. 12, no. 4, pp. 2470–2482, 2021, http://doi.org/10.11591/ijpeds.v12.i4.pp2470-2482.

[21] R. Rouabhi, R. Abdessemed, A. Chouder, and A. Djerioui, "Hybrid backstepping control of a doubly fed wind energy induction generator," *Hybrid backstepping control of a doubly fed wind energy induction generator*, vol. 11, no. 1, pp. 367–376, 2015, https://num.univ-msila.dz/DWE/public/attachements/2022/10/25/mediterranenpdf-374gdabb1666674875.pdf.

[22] R. K. Kumar and J. Choudhary, "Current source converter-based optimal power extraction and power control of a doubly fed induction generator (DFIG) using backstepping control," *Engineering Research Express*, vol. 6, no. 1, 2024, https://doi.org/10.1088/2631-8695/ad153d.

[23] A. Kasbi and A. Rahali, "Performance improvement of modern variable-velocity wind turbines technology based on the doubly-fed induction generator (DFIG)," *Materialstoday Proceedings*, vol. 45, pp. 5426–5432, 2021, https://doi.org/10.1016/j.matpr.2021.02.114.

[24] B. Peng, F. Zhang, J. Liang, L. Ding, Z. Liang, and Q. Wu, "Coordinated control strategy for the short-term frequency response of a DFIG-ES system based on wind speed zone classification and fuzzy logic control," *International Journal of Electrical Power & Energy Systems*, vol. 107, pp. 363–378, 2019, https://doi.org/10.1016/j.ijepes.2018.11.010.

[25] R. Antão, *Type-2 fuzzy logic: uncertain systems' modeling and control*, Springer, 2017, https://www.google.co.id/books/edition/Type_2_Fuzzy_Logic/QPQtDwAAQBAJ?hl=en&gbpv=0.

[26] Z. Civelek, "Optimization of fuzzy logic (Takagi-Sugeno) blade pitch angle controller in wind turbines by genetic algorithm," *Engineering Science and Technology, an International Journal*, vol. 23, no. 1, pp. 1–9, 2020, https://doi.org/10.1016/j.jestch.2019.04.010.

[27] A. V. Hemeyine, A. Abbou, N. Tidjani, M. Mokhlis, and A. Bakouri, "Robust takagi sugeno fuzzy models control for a variable speed wind turbine based a DFI-generator," *International Journal of Intelligent Engineering and Systems*, vol. 13, no. 3, pp. 90–100, 2020, https://doi.org/10.22266/ijies2020.0630.09.

[28] S. Qin, S. S. Ngu, and T. Zeng, "Optimal constant power control of wind turbine generators based on Takagi-Sugeno fuzzy model," *Alexandria Engineering Journal*, vol. 61, no. 8, pp. 5977–5982, 2022, https://doi.org/10.1016/j.aej.2021.11.024.

[29] M. S. Chabani *et al.*, "Takagi–Sugeno Fuzzy Logic Controller for DFIG Operating in the Stand-Alone Mode: Simulations and Experimental Investigation," *Arabian Journal for Science and Engineering*, vol. 48, no. 11, pp. 14605–14620, 2023, https://doi.org/10.1007/s13369-023-07704-0.

[30] A. A. Chhipa *et al.*, "Adaptive neuro-fuzzy inference system-based maximum power tracking controller for variable speed wecs," *Energies*, vol. 14, no. 19, p. 6275, 2021, https://doi.org/10.3390/en14196275.

[31] P. Kou, D. Liang, J. Li, L. Gao and Q. Ze, "Finite-Control-Set Model Predictive Control for DFIG Wind Turbines," *IEEE Transactions on Automation Science and Engineering*, vol. 15, no. 3, pp. 1004-1013, 2018, https://doi.org/10.1109/TASE.2017.2682559.

[32] G. F. Gontijo, T. C. Tricarico, B. W. França, L. F. da Silva, E. L. van Emmerik and M. Aredes, "Robust Model Predictive Rotor Current Control of a DFIG Connected to a Distorted and Unbalanced Grid Driven by a Direct Matrix Converter," *IEEE Transactions on Sustainable Energy*, vol. 10, no. 3, pp. 1380-1392, 2019, https://doi.org/10.1109/TSTE.2018.2868406.

[33] M. Abdelrahem and R. Kennel, "Efficient Direct Model Predictive Control for Doubly-Fed Induction Generators," *Electric Power Components and Systems*, vol. 45, no. 5, pp. 574–587, 2017, https://doi.org/10.1080/15325008.2017.1289572.

[34] A. J. Sguarezi Filho, A. L. De Oliveira, L. L. Rodrigues, E. C. M. Costa, and R. V. Jacomini, "A robust finite control set applied to the DFIG Power Control," *Electric Power Components and Systems*, vol. 6, no. 4, pp. 1692–1698, 2018, https://doi.org/10.1080/15325008.2017.1289572.

[35] A. J. Sguarezi Filho, A. L. de Oliveira, L. L. Rodrigues, E. C. M. Costa and R. V. Jacomini, "A Robust Finite Control Set Applied to the DFIG Power Control," *IEEE Journal of Emerging and Selected Topics in Power Electronics*, vol. 6, no. 4, pp. 1692-1698, 2018, https://doi.org/10.1109/JESTPE.2018.2833474.

[36] H. El Alami *et al.*, "Robust Finite Control-Set Model Predictive Control for Power Quality Enhancement of a Wind System Based on the DFIG Generator," *Energies*, vol. 16, no. 3, p. 1422, 2023, https://doi.org/10.3390/en16031422.

[37] K. A. Naik, C. P. Gupta, and E. Fernandez, "Design and implementation of interval type-2 fuzzy logic-PI based adaptive controller for DFIG based wind energy system," *International Journal of Electrical Power & Energy Systems*, vol. 115, p. 105468, 2020, https://doi.org/10.1016/j.ijepes.2019.105468.

[38] J. Pande, P. Nasikkar, K. Kotecha, and V. Varadarajan, "A review of maximum power point tracking algorithms for wind energy conversion systems," *Journal of Marine Science and Engineering*, vol. 9, no. 11, p. 1187, 2021, https://doi.org/10.3390/jmse9111187.

[39] Y. Wang, L. Zou, L. Ma, Z. Zhao, and J. Guo, "A survey on control for Takagi-Sugeno fuzzy systems subject to engineering-oriented complexities," *Systems Science & Control Engineering*, vol. 9, no. 1, pp. 334–349, 2021, https://doi.org/10.1080/21642583.2021.1907259.

[40] A. Ammar, B. Talbi, T. Ameid, Y. Azzoug, and A. Kerrache, "Predictive direct torque control with reduced ripples for induction motor drive based on T-S fuzzy speed controller," *Asian Journal of Control*, vol. 21, no. 4, pp. 2155–2166, 2019, https://doi.org/10.1002/asjc.2148.

[41] V. Yaramasu and B. Wu, *Model Predictive Control of Wind Energy Conversion Systems*, John Wiley & Sons, 2016, https://doi.org/10.1002/9781119082989.

[42] A. Aggoune, F. Berrezzek, and K. Khelil, "Finite-Control-Set Model Predictive Control (FCS-MPC) and Fuzzy Self-Adaptive PI Controller (FSA-PIC) for Wind Turbine System Based on DFIG," *Proceedings of the 2nd International Conference of Nanotechnology for Environmental Protection and Clean Energy Production*, vol. 45, pp. 327–338, 2024, https://doi.org/10.1007/978-981-97-1916-7_34.